PNAS RESEARCH ARTICLE | APPLIED PHYSICAL SCIENCES

Ice friction at the nanoscale

Łukasz Baran[a], Pablo Llombart[b], Wojciech Rżysko[a], and Luis G. MacDowell[c,1]

Edited by Peter Rossky, Rice University, Houston, TX; received June 6, 2022; accepted October 10, 2022

The origin of ice slipperiness has been a matter of great controversy for more than a century, but an atomistic understanding of ice friction is still lacking. Here, we perform computer simulations of an atomically smooth substrate sliding on ice. In a large temperature range between 230 and 266 K, hydrophobic sliders exhibit a premelting layer similar to that found at the ice/air interface. On the contrary, hydrophilic sliders show larger premelting and a strong increase of the first adsorption layer. The nonequilibrium simulations show that premelting films of barely one-nanometer thickness are sufficient to provide a lubricating quasi-liquid layer with rheological properties similar to bulk undercooled water. Upon shearing, the films display a pattern consistent with lubricating Couette flow, but the boundary conditions at the wall vary strongly with the substrate's interactions. Hydrophobic walls exhibit large slip, while hydrophilic walls obey stick boundary conditions with small negative slip. By compressing ice above atmospheric pressure, the lubricating layer grows continuously, and the rheological properties approach bulk-like behavior. Below 260 K, the equilibrium premelting films decrease significantly. However, a very large slip persists on the hydrophobic walls, while the increased friction on hydrophilic walls is sufficient to melt ice and create a lubrication layer in a few nanoseconds. Our results show that the atomic-scale frictional behavior of ice is a combination of spontaneous premelting, pressure melting, and frictional heating.

tribology | lubrication | slip | premelting | quasi-liquid layer

Significance

Sliding on ice is a familiar experience, but we still do not fully understand why is ice slippery. Faraday hypothesized that ice forms spontaneously a thin quasi-liquid layer on its surface, while Reynolds suggested that this layer could act as a lubricant. However, experimentally probing the structure of ice below a slider is extremely challenging. Here, we perform computer simulations of a slider on ice and obtain atomic-scale insight into ice friction. We find that, depending on their hydrophobicity, sliders can either stick or slip atop a nanometer-thick self-healing, self-lubricating quasi-liquid layer with properties similar to bulk undercooled water. This allows us to explain the low friction of ice using macroscopic laws borrowed from continuum hydrodynamics and lubrication theory.

The slipperiness of ice has been exploited since ancient times as a means of transportation in cold regions (1). But despite many advances in tribology (2–4), a first principles understanding on this very familiar property is still lacking (5). A hypothesis dating back to the 19th century is that a self-lubricating water film on the ice surface is formed due to pressure melting (6, 7). Spontaneous equilibrium premelting (8) and frictional heating (9) have also been invoked to explain ice friction. However, other authors disregard the significance of water lubrication altogether (10–13), while recent experiments support boundary or elastohydrodynamic models of friction (12–15). Experimental confirmation of interfacial premelting films in the order of the nanometer does not resolve the controversy (16–21), as it is arguable whether macroscopic hydrodynamics assumed in most theories (22–24) is obeyed at such small length scales (25). In fact, computer simulations of flow under confinement reveal consistent violation of the stick boundary condition and the significance of water slip (26–30), while studies of water sliding on ice and grain boundary friction suggest negative slip instead (31, 32).

Here, we report molecular dynamics simulations of ice sliding past an atomically smooth substrate. Our results show that an interfacial premelting film formed spontaneously upon compression or frictional heating exhibits hydrodynamic properties similar to bulk undercooled water. This illustrates that a hydrodynamic theory of Couette flow supplemented with slip boundary conditions can explain the friction of ice at smooth contacts.

Results

In our study, we simulate explicitly ice sliding past an atomically smooth substrate under pressure (Fig. 1). The ice sample consists of a large orthorhombic slab of water molecules (30 bilayers thick) modeled with the TIP4P/Ice force field and oriented in the direction of the basal surface (33). The slider is modeled as a rigid face-centered cubic arrangement of atoms directed along the (111) plane, with lattice parameters selected to make a perfect match with the ice surface.

The wall atoms interact with water oxygens via a Lennard-Jones potential. This allows us to tune the hydrophobicity of the substrate merely by changing the strength of wall–oxygen interactions. The quality of the substrate is monitored by measuring the

Author affiliations: [a]Department of Theoretical Chemistry, Institute of Chemical Sciences, Faculty of Chemistry, Maria-Curie-Sklodowska University in Lublin, 20-031 Lublin, Poland; [b]Departamento de Física Teórica de la Materia Condensada, Instituto Nicolás Cabrera, Universidad Autónoma de Madrid, 28049 Madrid, Spain; and [c]Departamento de Química-Física, Facultad de Ciencias Químicas, Universidad Complutense de Madrid, 28040 Madrid, Spain

Author contributions: L.G.M. designed research; L.B. performed research; P.L. and W.R. contributed new reagents/analytic tools; L.B. and L.G.M. analyzed data; and L.G.M. wrote the paper.

The authors declare no competing interest.

This article is a PNAS Direct Submission.

[1]To whom correspondence may be addressed. Email: lgmac@quim.ucm.es.

This article contains supporting information online at http://www.pnas.org/lookup/suppl/doi:10.1073/pnas.2209545119/-/DCSupplemental.

Published November 28, 2022.

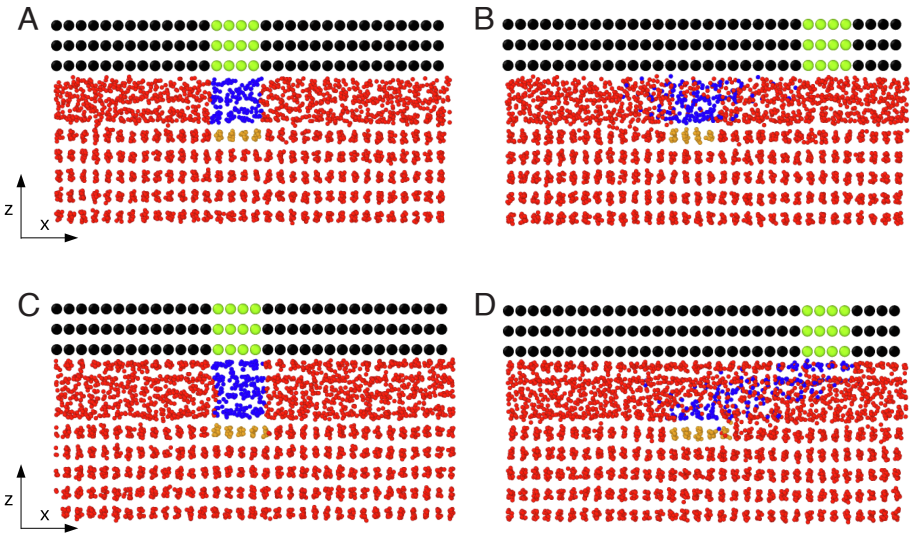

Fig. 1. Sliding on ice with atomic resolution. An imperfectly terminated ice slab gently compressed to $p = 1$ atm by an inert solid substrate at $T = 262$ K spontaneously develops a premelting film of thickness ca. $h = 1$ nm for both hydrophobic (*A*) and hydrophilic walls (*C*). The flow pattern after sliding over the equilibrated film with sliding velocity $U = 5$ m/s during 0.5 ns is illustrated by liquid-like molecules tagged in blue and wall atoms tagged in green color at $t = 0$. (*B*) For the hydrophobic substrate, the slider slips past the premelting film, and the liquid-like blue tagged molecules have hardly moved beyond their original position at $t = 0$ (Movie S1). (*D*) For the hydrophilic substrate, an adsorption layer sticks to the wall, and the premelting film is dragged by the slider with a pattern that resembles Couette flow (Movie S2). Solid-like orange colored molecules serve to illustrate stick boundary conditions at the ice/water interface and the exchange of solid and liquid molecules.

contact angle of water droplets, θ, which is varied in a range spanning both hydrophobic ($\theta = 120°$) and hydrophilic ($\theta = 50°$) walls (*SI Appendix, Text and Methods*).

Under skating conditions, the slider does not step on a perfectly terminated ice surface. Instead, the ice surface has been previously exposed to air and exhibits a significant premelting layer (31, 34–36). To mimic the contact of the slider with ice, we merely prepare the ice surface with a half-terminated bilayer and place it at a small distance from the substrate. The wall is then allowed to gently compress the slab to the desired pressure (see *Methods* section). At a temperature $T = 262$ K, somewhat lower but close to that of skating rinks, we find that a premelting film of the order of a nanometer thick evolves spontaneously and equilibrates in the scale of decades of nanoseconds for all substrates and pressures studied. The presence of premelting is obvious in the snapshots of Fig. 1 as a layer of disordered water molecules between the ordered bulk ice and the substrate. In the density profiles of Fig. 2 *A*–*D*, the signature of premelting is the emergence of density peaks that have lost the bilayer structure typical of bulk ice that is apparent within the bulk region. This is confirmed by use of the CHILL+ order parameter (37), which allows to resolve solid-like from liquid-like water molecules (*SI Appendix, Methods*).

After equilibration, we model sliding by moving the top and bottom sliders with equal sliding speed $U = 5$ m/s and opposite direction. Although the properties of premelting layers of ice exposed to vacuum are often invoked as a proxy to explain ice friction (5, 12, 31), inspection of simulation snapshots shows a dramatic dependence of the sliding dynamics on the substrate interactions. Here, we describe results obtained at ambient pressure $p = 1$ atm and $T = 262$ K (Fig. 1 and Movies S1 and S2), but similar results are found in all the temperature range from 230 to 266 K (*SI Appendix*, Figs. S1 and S2).

For the hydrophobic substrate, $\theta = 120°$, the slider slips past the premelting film and generates an extremely small velocity field. Molecules tagged in blue in Fig. 1*A* at $t = 0$ have diffused almost equally in both directions after a sliding time of 0.5 ns (Fig. 1*B*); i.e., as observed in the flow of water inside carbon nanotubes (26, 28, 30, 38), friction is extremely small, and the premelting film is hardly susceptible to the motion of the slider. On the contrary, for the hydrophilic substrate, with $\theta = 50°$, an adsorbed layer of water molecules next to the substrate at $t = 0$ (Fig. 1*C*) sticks to the wall and is displaced by the same amount as the slider after 0.5 ns (Fig. 1*D*). The remaining blue tagged molecules in the premelting film are loosely dragged by the slider and display clear hints of Couette flow.

The large difference in the frictional behavior can be anticipated from the plot of equilibrium density profiles (39). Here, we describe results obtained at $T = 262$ K (Fig. 2 *A*–*D*), but the same trend is observed in all the temperature range studied (*SI Appendix*, Figs. S3 and S4). For the hydrophobic substrate ($\theta = 120°$), the structure of the premelting film is very similar to that found when the ice surface is exposed to vacuum (green dashed line in Fig. 2*A*). The density profiles differ significantly only by the presence of a small density peak that appears in the confined film close to the wall. However, increasing the strength of the wall interactions results in an increase of the film thickness and the appearance of a strongly layered liquid film. Particularly, we see a large enhancement of the first adsorption peak, with a density that can increase as much as a factor of three compared to that observed in the hydrophobic wall with $\theta = 120°$ (Fig. 2*D*). By visual inspection, we confirm that the water molecules pertaining to the first adsorption peak exhibit strong intralayer hydrogen bonding, with proliferation of flattened hexagonal rings as observed in adsorbed thin films on metals (40, 41), and undercooled water under confinement (42, 43).

We expect the hydrogen bond network on the first adsorption peak of hydrophilic substrates to have a significant impact on the mobility of water molecules (31, 34, 39). To show this, we divide the premelting film into regions that allow us to single out the wall adsorption layer from the ice adsorption layer, as illustrated with vertical dashed lines in Fig. 2 *A*–*D*. For each of these two regions, we estimate an effective parallel self-diffusion coefficient, $D_{\parallel}$, by measuring the tangential mean squared displacement of the

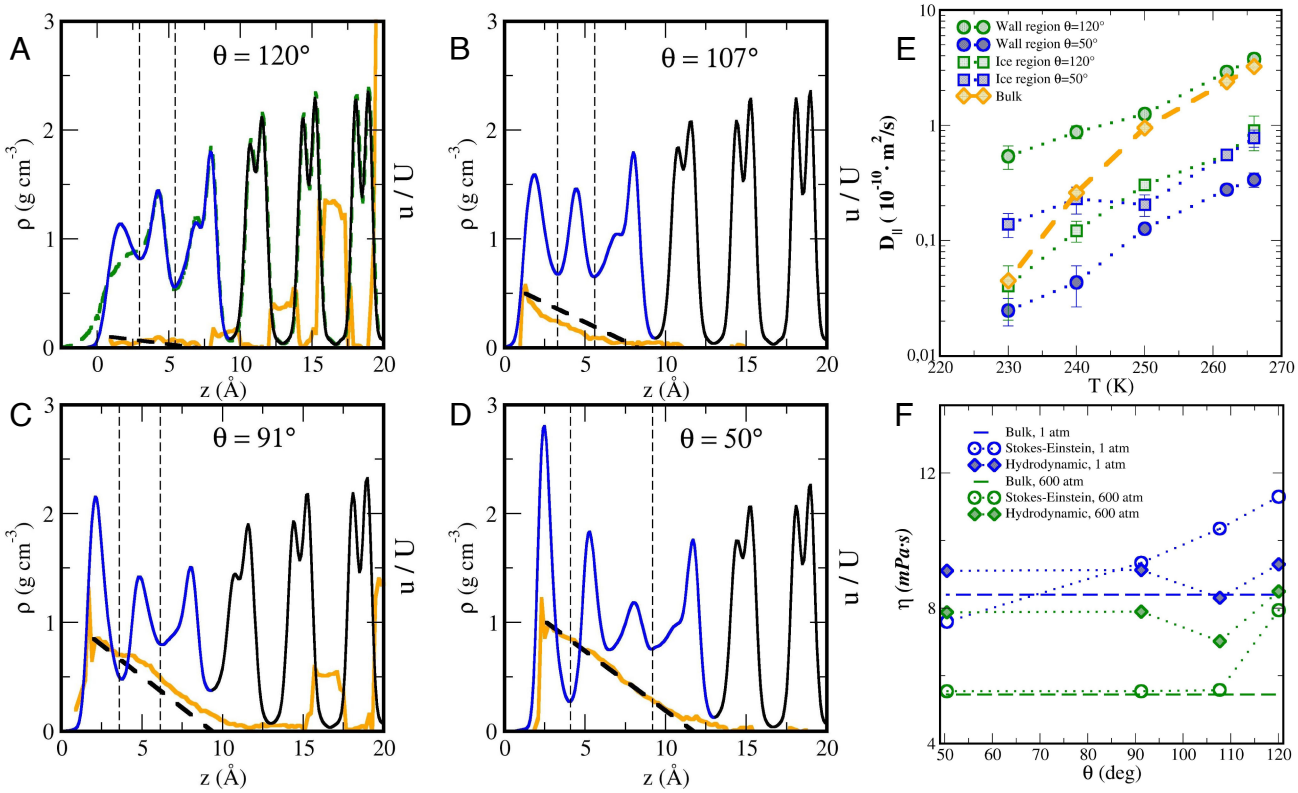

Fig. 2. Structure and dynamics of premelted films during sliding. Panels (*A, B, C, and D*) show equilibrium density profiles and velocity profiles for a sliding experiment at $p = 1$ atm, $T = 262$ K, and $U = 5$ m/s during 10 ns. The total density profile (left axis) is shown as a continuous line, with blue color for the region where liquid-like water is the majority phase and black color where ice is the majority phase. The premelting film is divided into a wall–adsorbed layer, an ice–adsorbed layer, and a central quasi-bulk region, as illustrated by vertical dashed lines. Panel (*A*) also shows the total density of a premelting film for ice in contact with a vacuum (green dashed line). The thick orange lines display the velocity profile in units of the sliding velocity (right axis, with tick marks as displayed in the left axis). The dashed black line is the hydrodynamic flow profile predicted from the model of Eq. **1**. Panels correspond to different wall interactions: (*A*) Hydrophobic wall, with $\theta = 120°$, (*B*) $\theta = 107°$, (*C*) $\theta = 91°$. (*D*) Hydrophilic wall with $\theta = 50°$. Panel (*E*): Diffusivity at the wall and ice adsorption layers as a function of temperature. The orange diamonds stand for the bulk diffusion coefficients at $p = 1$ atm. The remaining symbols correspond to parallel diffusion coefficients of the wall–adsorption layer (circles) and the ice–adsorption layer (squares); Green symbols stand for the hydrophobic wall with $\theta = 120°$ and blue symbols for the hydrophilic wall with $\theta = 50°$. Panel (*F*): Quasi-bulk-like viscosity of the premelting film. The thick dashed line displays the shear viscosity of bulk undercooled water as determined from Green–Kubo calculations. The circles display viscosities as determined from the Stokes–Einstein relation using the parallel diffusion coefficient calculated in the central quasi-bulk-like region of the premelting films. The diamonds are hydrodynamic viscosities as determined from the film thickness and shear stress of the simulations. Results are shown for $T = 262$ K, with $p = 1$ atm (blue) and $p = 600$ atm (green).

water-like molecules in that region (Fig. 2*E*). Our results confirm a dramatic impact of the wall–water interactions on the mobility of the wall–adsorption layer. For the hydrophobic substrate, $\theta = 120°$, the parallel diffusion coefficient is somewhat larger than that of bulk undercooled water for most temperatures studied, as observed in premelting films exposed to vacuum (12, 31, 34), and becomes an order of magnitude larger on approaching 230 K. However, for the hydrophilic substrate, $\theta = 50°$, the diffusion coefficient of the wall–adsorption layer remains one order of magnitude smaller than that of the hydrophobic substrate all the way from 266 to 230 K. On the other hand, for the ice–adsorption layer, the diffusion coefficient remains small and almost independent of θ, implying that the details of the slider do not impact the friction of premelted water at the ice interface.

For temperatures above 260 K, the premelting layer develops a well-defined quasi-bulk region between the adsorption layers, as observed in Fig. 2 and *SI Appendix*, Figs. S3 and S4. Our results show that the parallel diffusion coefficient in this central region is somewhat smaller, but of the same order of magnitude as the diffusion coefficient of bulk water, even for the films studied here, which are barely 1 nm thick (26) (*SI Appendix*, Fig. S5). This is in agreement with measurements of mobility in confined water (21, 26, 44, 45) and suggests that large effective viscosities measured in mechanical tests (14) might not be related to the actual hydrodynamics of the premelting film, as noticed in ref. 21. This is not in conflict with the observation of anomalous diffusion at grain boundaries, which is related to the attachment/detachment of water molecules into the ordered ice lattice due to motion in the perpendicular direction (46). We find that in the time scale of about 2–8 ns in which premelted water molecules remain within the central quasi-bulk region of the premelting film, the mobility in the parallel direction remains close to bulk-like. This suggests that the central region within the premelting film will exhibit shearing similar to that observed in bulk undercooled water. As a hint, we notice that the viscosity predicted from the Stokes–Einstein relation $\eta_{SE} = k_B T / 6\pi D_{\parallel} a$, with $a = 0.155$ nm describing the molecular radius of a water molecule, provides an order of magnitude approximation to the viscosity of undercooled water calculated independently at $T = 262$ K and $p = 1$ atm from bulk simulations (Fig. 2*F*).

In practice, sliding occurs at contact with surface asperities, and the pressure on the contact zone can well reach several hundred atmospheres (9, 12, 13, 15, 23, 24). However, increasing pressure drives ice closer to the melting line. Therefore, the thickness of the premelting film is expected to increase. We confirm this by compressing our confined ice slabs and estimating

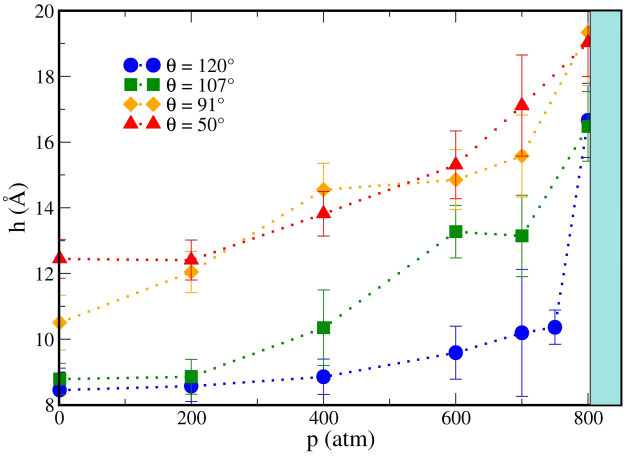

Fig. 3. Increasing equilibrium premelting thickness by compression. Results display the equilibrium interfacial premelting thickness as a function of pressure for different substrates at $T = 262$ K. Blue circles: $\theta = 120°$; green squares: $\theta = 107°$; orange triangles: $\theta = 91°$; red triangles: $\theta = 50°$. The hashed region displays the estimated melting pressure for the model.

the equilibrium film thickness as $h_{eq} = \Gamma_w/\rho_w$, with Γ_w, the number of liquid-like molecules per unit surface, and ρ_w, the bulk liquid density. The results of Fig. 3 show that, independent of the substrate quality, the interfacially premelted films increase their thickness under compression, showing that pressure melting and interfacial premelting are inextricably entangled (16, 18).

As a result of this surface-pressure melting, the diffusion coefficient and the corresponding Stokes–Einstein viscosity of the films approach bulk-like conditions as illustrated in *SI Appendix*, Fig. S5 and Fig. 2*F* for interfacially premelted films compressed at a pressure of $p = 600$ atm.

In order to check how bulk like is the sliding hydrodynamics of a quasi-liquid layer barely one nanometer thick, we study the shear response of the premelting film upon sliding the wall with a constant lateral velocity $U = 5$ m/s at $T = 262$ K and $p = 1$ atm for a period of 10 ns (Fig. 2 *A–D*). Similar calculations are performed for $p = 600$ atm (*SI Appendix*, Fig. S6) and $p = 1$ atm in the temperature range 230–266 K (*SI Appendix*, Figs. S3 and S7).

Averaging the velocity components in the x direction parallel to the slider, we obtain the hydrodynamic flow profile $u(z)$ as a function of the perpendicular distance to the wall. For the hydrophobic wall (Fig. 2*A*), $u(z)$ is hardly distinguishable from thermal motion (28). It appears as a noisy curve with very small positive velocity that hardly attains 10% of the total wall velocity. However, as the wall hydrophilicity begins to increase (Fig. 2 *B–D*), a roughly linear flow profile appears that strongly resembles expectations from a model of simple Couette flow with partial slip (2, 28, 38, 47, 48). By visual inspection, we can define σ_1 as the position close to the wall adsorption peak where the approximately linear flow profile attains its maximal velocity, $u_s = u(z = \sigma_1)$. Similarly, we define σ_2, close to the ice adsorption peak, where the extrapolated flow profile vanishes, $u(z = \sigma_2) = 0$ (*SI Appendix*, Fig. S8 and Tables S1 and S2). Interestingly, we find that σ_2 is at about one molecular diameter away from the first ice bilayer, in agreement with reports of a small negative slip length for water flow past bulk ice (49).

If the hydrodynamics of the premelting film follows a model of Couette flow, we expect that the shear stress, τ, should obey $\tau = \eta \frac{u_s}{d_C}$ (2, 3, 48), where u_s is the slip velocity, $u_s = u(z = \sigma_1)$, d_C is the thickness of the region where the actual Couette flow takes place, and η is the bulk viscosity. To check this, we calculate the effective hydrodynamic viscosity as $\eta_H = \tau d_C/u_s$, with τ measured from the force exerted by the wall on the premelting film, $d_C = \sigma_2 - \sigma_1$, and u_s estimated by visual inspection of the flow profile. The results for η_H are shown in Fig. 2*F* and appear barely 10% above the viscosity of bulk water. Alternatively, we can assume that the premelting film behaves as bulk water and obtain a hydrodynamic film thickness as $d_H = \eta u_s/\tau$, with η being the bulk viscosity (38). We checked that the value thus obtained agrees within ±0.3 nm with the estimated Couette thickness, d_C. Now, using d_H, and u_s, we can obtain a synthetic Couette flow profile under the assumption that $u(z) = u_s$ at $z = \sigma_1$ and vanishes at $z = \sigma_1 + d_H$. The resulting model is displayed in Fig. 2 *A–D* together with the actual velocity profiles measured in the simulations. A qualitative agreement is obvious for substrates $\theta = 107°$ and $\theta = 91°$ and is almost as good as a linear regression for the hydrophilic substrate with $\theta = 50°$ (similar good agreement is found also for $p = 600$ atm, *SI Appendix*, Fig. S6 and $T = 266$ K, *SI Appendix*, Figs. S3 and S7). As a rule of thumb, we see that the Couette flow is established between the wall and ice adsorption layers of liquid-like water, so that the location of the hydrodynamic boundary conditions may be inferred with little cost from equilibrium simulations.

Put together, our results strongly support that the shear force of the slider on thin premelting films hardly one nanometer thick may be described approximately by a very simple model of Couette flow with slip:

$$\tau = \frac{\eta U}{h_H + b}, \qquad [1]$$

where $h_H = \sigma_1 + d_H$ is the hydrodynamic film thickness, b is a slip length and η is an effective viscosity similar to the viscosity of undercooled bulk water (*SI Appendix*, Fig. S8). We test the consistency of the model by performing additional simulations at a smaller sliding velocity $U = 0.5$ m/s and find that the calculated shear force is about 10 times smaller than that measured at $U = 5$ m/s, consistent with Eq. **1** (*SI Appendix*, Table S3).

We can estimate a Couette slip length b_C for use in Eq. **1** directly from visual inspection of the velocity profile of Fig. 2 *A–D*, noticing that $U/(d_C + \sigma_1 + b_C) = u_s/d_C$. A figure of the slip length as a function of wall strength illustrates the large difference of frictional behavior. For $\theta = 120°$, b_c is about five times larger than the actual film thickness, consistent with observations of giant slip lengths in confined undercooled water and water at hydrophobic substrates (26, 30). As the wall strength increases, however, the slip length decreases fast and becomes negative for hydrophilic walls, illustrating a large impact of wall interactions on the early stages of ice friction (Fig. 4).

To further check the consistency of the model, we can invoke the Navier slip boundary condition, which assumes a shear stress proportional to the velocity drop at the hydrodynamic boundary, i.e., $\tau = \lambda(U - u_s)$, where $\lambda = \eta/b$ is the interfacial friction coefficient (27, 28, 38, 48). Combining these equations, we estimate a hydrodynamic slip length $b_H = (U - u_s)\eta/\tau$ by using the shear stress obtained in the simulations, u_s from the velocity profile, and η the viscosity of bulk water. The results in Fig. 4 show remarkable good agreement with the Couette slip length measured previously and attest to the accuracy of Eq. **1** as a valid model for the shear stress of atomically smooth sliders on ice.

Since increasing the temperature or pressure increases the equilibrium film thickness, Eq. **1** is expected to hold everywhere above $T = 262$ K and $p = 1$ atm. At lower temperature, however,

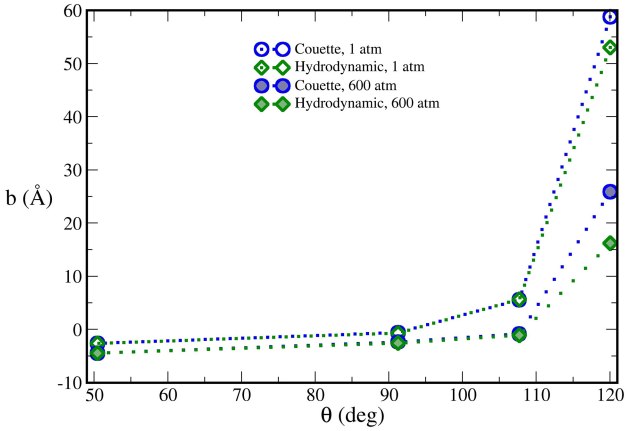

Fig. 4. Slip and stick boundary conditions of premelted films. As wall hydrophilicity increases, the premelting film dynamics evolves from large to negative slip. Blue circles are Couette slip lengths, with b_C estimated from the average flow profile. Green diamonds are hydrodynamic slip lengths, with b_H calculated from the shear force.

SI Appendix, Figs. S3 and S4 show that the premelting films consist of at most two adsorption layers and no quasi-bulk region at all. This drives the system fully into the boundary friction regime. Surprisingly, the ice surface remains slippery for both hydrophobic and hydrophilic sliders. Indeed, using our results for the shear stress from the nonequilibrium simulations (*SI Appendix*, Tables S3 and S4), and indentation hardness results for the applied load (13), we find order of magnitude agreement with experimental friction coefficients in all the temperature range studied (*SI Appendix*, *Text* and Fig. S9). The origin of the small friction coefficients varies greatly with hydrophilicity, however. In the case of hydrophobic sliders, the diffusion coefficient of the adsorption layer remains always larger than the bulk diffusion coefficient (Fig. 2*E*) and allows for a very large slip (*SI Appendix*, Figs. S1 and S2), as suggested in ref. 12. For hydrophilic sliders, on the contrary, shear is sufficiently large to melt one full bilayer in barely 0.5 ns due to frictional heating. As a result, an equilibrium premelting film consisting of one single adsorption layer attains nanometer thickness in less than 5 ns (*SI Appendix*, Fig. S1 and Movie S3). Therefore, hydrophilic sliders develop a layer that is sufficiently thick to achieve lubrication, even at low temperature. This is visible in the close-to-linear velocity profiles observed in *SI Appendix*, Fig. S7. However, for a nanometer-thick film at the large sliding speeds $U = 5$ m/s that we study, the shear rate $\dot{\gamma} = U/d$ attains the scale of $5 \cdot 10^9$ s^{-1}. Above 262 K, this is still small, and the lubrication layer exhibits Newtonian flow. However, as the temperature decreases, this becomes well above the threshold of non-Newtonian flow (50). Indeed, from the velocity profiles of Fig. S7, we find hydrodynamic viscosities that become up to two orders of magnitude smaller than the bulk viscosity at $T = 230$ K. The shear rate-dependent viscosities so obtained roughly follow the Eyring model of shear thinning (*SI Appendix*, *Text* and Fig. S10). Interestingly, the hydrophilic sliders at low temperature display a small elastic deformation (Movie S3), but this accounts only for a few percent of the total shear stress (*SI Appendix*, *Text*).

Discussion

In practice, ice friction is a multiscale problem, and both the slider and ice are atomically rough (4, 51). As a result, it is thought that most of the slider's load is supported locally in high-pressure zones (9, 12, 13, 15, 23, 24). In conventional applications, low-viscosity liquids such as water behave as very poor lubricants because the large pressure between asperities squeezes out the lubrication film, resulting in bare contact friction (2, 3, 13, 15, 23). This argument was used recently by Canale et al. (14) and Bonn et al. (12, 13) to put into question the role of premelting-mediated lubrication in ice friction. Our results show that ice does not behave as an ordinary inert substrate. Increasing the pressure drives it closer to the melting line and leads to an increase of the equilibrium premelting thickness (Fig. 3). Of course, a high contact pressure will conspire to squeeze out the lubrication film (52). By Le Chatelier's principle, however, ice will melt in order to restore the equilibrium thickness (16, 18, 53). Due to this self-healing property of the premelting film, we expect that lubrication will be enhanced at high pressure.

Based on these considerations, and the model of Eq. **1**, we find that the friction coefficient of an atomically smooth region on the ice/slider system should obey $\mu_f = \frac{\eta(\dot{\gamma})U}{(h_H+b)p}$, where p is the pressure of the high-pressure zone (23, 24).

At $T = 262$ K, moderate sliding speeds of the order of mm/s, assumed film thicknesses of ca. 1 nm and zero slip, this gives already small friction coefficients at a pressure of one atm, ca. $\mu_f = 0.1$. Considering instead that the sliding contact is exercised at the indentation hardness limit of ca. $p = 100$–1000 atm (11–13, 24), we obtain friction coefficients two to three orders of magnitude smaller. Increasing the sliding velocity to the m/s range yields higher estimates of order $\mu_f \approx 1$, well away from experimental measurements. However, at such ranges, friction inputs heat at a large rate of $\eta U^2/(h_H + b)$ ca. 35–200 MJ/m^2 s, which is sufficient to melt roughly one full bilayer in the scale of nanoseconds. Unless heat is dissipated within the slider at a very fast rate, this will result in a large increase of the film thickness within a few hundred nanoseconds, as assumed tacitly in current theories of frictional heating (23, 24). Indeed, we can see in our 10 ns sliding simulations clear evidence of bilayer melting at temperatures as low as 230 K, despite the use of a thermostat (Movie S3).

Our model is also consistent with the temperature dependence observed for the friction coefficient (9–13). For hydrophobic walls at low temperature, the slip length becomes very large (30), and the lubrication model with slip yields $\mu_f = \lambda U/p$, where λ is the interfacial friction (48). For undercooled water, $\lambda(T)$ follows an anti-Arrhenius behavior (30) that is consistent with a large increase of μ_f with decreasing temperature (10–13). The result $\mu_f = \lambda U/p$ also explains the velocity strengthening observed for the friction coefficient at slow velocities (11, 13, 54). At larger sliding velocities, shear thinning becomes significant. This leads to a friction coefficient with a weaker, logarithmic dependence on the sliding speed, $\mu_f \propto \ln(U)/p$ (*SI Appendix*, *Text*). When the pressure is equated to the indentation hardness, which increases faster than $\ln(U)$ (13), this results in the velocity weakening of the friction coefficient found in experiments (9–11, 13, 54).

Overall, we find that our results lend strong support to the hypothesis of lubricated ice friction that has been put into question in recent experiments based on millimeter scale probes (12–14). Contrary to findings by Canale et al. (14), for corrugated probes, our results suggest that at atomically smooth contacts, the effective viscosity η is a meaningful and well-defined parameter, on the order of the bulk viscosity, which exhibits shear thinning at low temperature. Unlike suggestions by Weber et al. (12), the

dependence of ice friction on the substrate's slip length b shows that the sliding dynamics cannot be generally correlated with the properties of premelting films at the ice/vapor interface, except for highly hydrophobic sliders.

We emphasize, however that our results describe the frictional behavior at atomically smooth contacts. At a larger scale, both the slider and ice exhibit microscale roughness, and the total load of the slider is supported by a small amount of asperities. Accordingly, the friction coefficient is not only given by the shear at the smooth contacts but also by the indentation hardness of ice, which sets the fractional area supporting the slider's load (11–13, 24). At a larger scale, the formation of a slurry of water and ice could result in a very complex viscoelastic response (14, 15).

In summary, we have shown that a very small extent of interfacial premelting in ice provides a lubricating quasi-liquid layer that can be described close to quantitatively by a model of bulk Couette flow with slip. The premelted layer can further grow by compression and frictional heating. Our results reconcile the long-standing controversy on the origin of ice slipperiness and show that equilibrium premelting, pressure melting, and frictional heating operate simultaneously.

Materials and Methods

Computer Simulations. Molecular dynamics simulations in the Np_zAT ensemble were performed using LAMMPS (55). Trajectories were evolved with the velocity-Verlet algorithm, with a time step of 2 fs. Bonds and bond angles were constrained by the use of the SHAKE algorithm. The temperature was set using the velocity rescale algorithm with damping factor $\tau = 0.2$ ps (56). The pressure was set by applying a constant normal force $F_z = \pm p_z A/N_w$ directed in the direction of bulk ice on each of the N_w wall atoms (29, 30, 38). This avoids perturbation of the dynamics that is usual in conventional barostats. To prevent strain effects in the parallel direction, the lattice parameters are set to the equilibrium value at pressure p_z. Shear was imposed on ice by moving the walls tangentially in the x direction at a constant sliding speed (with opposite direction on each wall) (2, 32, 38, 48). All Lennard-Jones interactions were truncated beyond 1 nm. Electrostatic interactions were evaluated with a particle–particle particle–mesh solver. The charge structure factors were evaluated with a grid spacing of 1 Å and a fourth-order interpolation scheme. It resulted in $36 \times 32 \times 120$ ($72 \times 64 \times 120$ during Couette flow simulations) vectors in the x, y, z reciprocal directions, respectively. In the nonequilibrium simulations, equilibrated bulk systems were replicated by a factor of two on each of the parallel directions to gather sufficient statistics for the flow profile, and the thermostat was set only in the directions perpendicular to the flow, using a damping factor $\tau = 1$ ps. Shear was imposed on ice by moving the walls tangentially in the x direction at a constant sliding speed for 10 ns (with opposite direction on each wall). The averages were collected over 10 independent runs. Further details on the simulation setup and analysis may be found in *SI Appendix, Methods* and Figs. S11–S15.

Data, Materials, and Software Availability. All study data are included in the article and/or *SI Appendix*.

ACKNOWLEDGMENTS. We would like to thank Eva G. Noya for providing us with a code for the CHILL+ order parameter and G. de Vilhena for careful reading of the manuscript. We would also like to thank Steve Plimpton for help with LAMMPS. We acknowledge funding from the Spanish Agencia Estatal de Investigación under research grant PIP2020-115722GB-C21. PL also thanks Ministerio de Ciencia e Innovacion for financial support under a Juan de la Cierva fellowship FJC2019-041329-I.

1. J. Li, H. Chen, H. A. Stone, Ice lubrication for moving heavy stones to the forbidden city in 15th- and 16th-century china. *Proc. Natl. Acad. Sci. U.S.A.* **110**, 20023–20027 (2013).
2. M. O. Robbins, M. H. Müser, *Computer simulations of friction, lubrication and wear in Modern Tribology Handbook* (CRC-Press, Boca Ratón, 2000).
3. B. N. J. Persson, *Sliding Friction: Physical Principles and Applications* (Springer-Verlag, Berlin, 2000).
4. A. Vanossi, N. Manini, M. Urbakh, S. Zapperi, E. Tosatti, Colloquium: Modeling friction: From nanoscale to mesoscale. *Rev. Mod. Phys.* **85**, 529–552 (2013).
5. R. Rosenberg, Why is ice slippery? *Phys. Today* **58**, 50–55 (2005).
6. B. E. Joly, Phenomena of skating, and Professor J. Thomson's thermodynamic relation. *Sci. Proc. R. Dublin Soc* **5**, (1886).
7. O. Reynolds, On the slipperiness of ice. *Mem. Proc. Manchester Lit. Phil. Soc.* **83**, 1–7 (1899).
8. H. Jellinek, Liquid-like (transition) layer on ice. *J. Colloid. Interface Sci.* **25**, 192–205 (1967).
9. F. P. Bowden, Friction on snow and ice. *Proc. R. Soc. Lond. A* **217**, 462–478 (1953).
10. S. Budnevich, B. Derjaguin, On the slip of solids on ice. *Prog. Surf. Sci.* **45** (1), 262–276 (1994).
11. K. Tusima, "Adhesion theory for low friction on ice" in *New Tribological Ways*, T. Ghrib, Ed. (IntechOpen, Rijeka, 2011).
12. B. Weber *et al.*, Molecular insight into the slipperiness of ice. *J. Phys. Chem. Lett.* **9**, 2838–2842, PMID: 29741089 (2018).
13. R. W. Liefferink, F. C. Hsia, B. Weber, D. Bonn, Friction on ice: How temperature, pressure, and speed control the slipperiness of ice. *Phys. Rev. X* **11** (2021).
14. L. Canale *et al.*, Nanorheology of interfacial water during ice gliding. *Phys. Rev. X* **9** (2019).
15. J. H. Lever *et al.*, Revisiting mechanics of ice-skate friction: from experiments at a skating rink to a unified hypothesis. *J. Glaciol.* 1–20 (2021).
16. J. G. Dash, History of the search for continuous melting. *Rev. Mod. Phys.* **71**, 1737–1743 (1999).
17. D. Beaglehole, P. Wilson, Extrinsic premelting at the ice-glass interface. *J. Chem. Phys.* **98**, 8096–8100 (1994).
18. J. S. Wettlaufer, "Crystal growth, surface phase transitions and thermomolecular pressure" in *Ice Physics and the Natural Environment*, J. S. Wettlaufer, J. G. Dash, Eds. (Springer-Verlag, Berlin, 1999), vol. 56, pp. 39–67.
19. S. Engemann *et al.*, Interfacial melting of ice in contact with sio_2. *Phys. Rev. Lett.* **92** (2004).
20. J. F. D. Liljeblad, I. Furó, E. C. Tyrode, The premolten layer of ice next to a hydrophilic solid surface: correlating adhesion with molecular properties. *Phys. Chem. Chem. Phys.* **19**, 305–317 (2017).
21. H. Li *et al.*, Water mobility in the interfacial liquid layer of ice/clay nanocomposites. *Angew. Chem. Int. Ed.* **60**, 7697–7702 (2021).
22. P. Oksanen, J. Heikonen, The mechanism of friction of ice. *Wear* **78**, 315–324 (1982).
23. S. Colbeck, The kinetic friction of snow. *J. Glaciol.* **34**, 78–86 (1988).
24. E. Lozowski, K. Szilder, S. A. Maw, A model of ice friction for a speed skate blade. *Sports Eng.* **16**, 239–253 (2013).
25. M. Majumder, N. Chopra, R. Andrews, J. HB, Enhanced flow in carbon nanotubes. *Nature* **438**, 44 (2005).
26. K. Falk, F. Sedlmeier, L. Joly, R. R. Netz, L. Bocquet, Molecular origin of fast water transport in carbon nanotube membranes: Superlubricity versus curvature dependent friction. *Nano Lett.* **10**, 4067–4073, PMID: 20845964 (2010).
27. J. S. Hansen, B. D. Todd, P. J. Daivis, Prediction of fluid velocity slip at solid surfaces. *Phys. Rev. E* **84**, 016313 (2011).
28. S. K. Kannam, B. D. Todd, J. S. Hansen, P. J. Daivis, How fast does water flow in carbon nanotubes? *J. Chem. Phys.* **138**, 094701 (2013).
29. S. Di Lecce, A. A. Kornyshev, M. Urbakh, F. Bresme, Electrotunable lubrication with ionic liquids: the effects of cation chain length and substrate polarity. *ACS Appl. Mater. Interfaces* **12**, 4105–4113, PMID: 31875392 (2020).
30. C. Herrero, G. Tocci, S. Merabia, L. Joly, Fast increase of nanofluidic slip in supercooled water: The key role of dynamics. *Nanoscale* **12**, 20396–20403 (2020).
31. P. B. Louden, J. D. Gezelter, Why is ice slippery? simulations of shear viscosity of the quasi-liquid layer on ice. *J. Phys. Chem. Lett.* **9**, 3686–3691, PMID: 29916247 (2018).
32. I. de Almeida Ribeiro, M. de Koning, Grain-boundary sliding in ice ih: Tribology and rheology at the nanoscale. *J. Phys. Chem. C* **125**, 627–634 (2021).
33. J. L. F. Abascal, E. Sanz, R. G. Fernandez, C. Vega, A potential model for the study of ices and amorphous water: TIP4P/Ice. *J. Chem. Phys.* **122**, 234511. (2005).
34. T. Kling, F. Kling, D. Donadio, Structure and dynamics of the quasi-liquid layer at the surface of ice from molecular simulations. *J. Phys. Chem. C* **122**, 24780–24787 (2018).
35. P. Llombart, E. G. Noya, L. G. MacDowell, Surface phase transitions and crystal habits of ice in the atmosphere. *Sci. Adv.* **6**, (2020).
36. B. Slater, A. Michaelides, Surface premelting of water ice. *Nat. Rev. Chem.* **3**, 172–188 (2019).
37. A. H. Nguyen, V. Molinero, Identification of clathrate hydrates, hexagonal ice, cubic ice, and liquid water in simulations: The chill+ algorithm. *J. Phys. Chem. B* **119**, 9369–9376 (2015).
38. C. Herrero, T. Omori, Y. Yamaguchi, L. Joly, Shear force measurement of the hydrodynamic wall position in molecular dynamics. *J. Chem. Phys.* **151**, (2019).
39. V. M. Nikiforidis, S. Datta, M. K. Borg, R. Pillai, Impact of surface nanostructure and wettability on interfacial ice physics. *J. Chem. Phys.* **155**, 234307 (2021).
40. J. Carrasco, A. Hodgson, A. Michaelides, A molecular perspective of water at metal interfaces. *Nature Mat.* **11**, 667–674 (2012).
41. T. K. Shimizu, S. Maier, A. Verdaguer, J. J. Velasco-Velez, M. Salmeron, Water at surfaces and interfaces. *Prog. Surf. Sci.* **93**, 87–107, Special Issue in Honor of Prof. Maki Kawai (2018).
42. N. Kastelowitz, J. C. Johnston, V. Molinero, The anomalously high melting temperature of bilayer ice. *J. Chem. Phys.* **132**, 124511 (2010).
43. C. Zhu *et al.*, Direct observation of 2-dimensional ices on different surfaces near room temperature without confinement. *Proc. Natl. Acad. Sci. U.S.A.* **116**, 16723–16728 (2019).
44. J. G. Dash, H. Fu, J. S. Wettlaufer, The premelting of ice and its environmental consequences. *Rep. Prog. Phys.* **58**, 115–167 (1995).
45. Y. Xu, N. G. Petrik, R. S. Smith, B. D. Kay, G. A. Kimmel, Growth rate of crystalline ice and the diffusivity of supercooled water from 126 to 262 k. *Proc. Natl. Acad. Sci. U.S.A.* **113**, 14921–14925 (2016).
46. P. A. F. P. Moreira *et al.*, Anomalous diffusion of water molecules at grain boundaries in ice ih. *Phys. Chem. Chem. Phys.* **20**, 13944–13951 (2018).
47. P. A. Thompson, M. O. Robbins, Shear flow near solids: Epitaxial order and flow boundary conditions. *Phys. Rev. A* **41**, 6830–6837 (1990).
48. J. L. Barrat, L. Bocquet, Influence of wetting properties on hydrodynamic boundary conditions at a fluid/solid interface. *Faraday Discuss.* **112**, 119–128 (1999).

49. P. B. Louden, J. D. Gezelter, Friction at ice-ih/water interfaces is governed by solid/liquid hydrogen-bonding. *J. Phys. Chem. C* **121**, 26764–26776 (2017).
50. I. de Almeida Ribeiro, M. de Koning, Non-newtonian flow effects in supercooled water. *Phys. Rev. Res.* **2**, 022004 (2020).
51. M. H. Müser *et al*., Meeting the contact-mechanics challenge. *Tribol. Lett.* **65**, 118 (2017).
52. B. Pittenger *et al*., Premelting at ice-solid interfaces studied via velocity-dependent indentation with force microscope tips. *Phys. Rev. B* **63**, 134102 (2001).
53. D. N. Sibley, P. Llombart, E. G. Noya, A. J. Archer, L. G. MacDowell, How ice grows from premelting films and liquid droplets. *Nat. Commun.* **12**, 239 (2021).
54. E. M. Schulson, A. L. Fortt, Friction of ice on ice. *J. Geophys. Res. Solid Earth* **117** (2012).
55. A. P. Thompson *et al*., LAMMPS - a flexible simulation tool for particle-based materials modeling at the atomic, meso, and continuum scales. *Comp. Phys. Comm.* **271**, 108171 (2022).
56. G. Bussi, D. Donadio, M. Parrinello, Canonical sampling through velocity rescaling. *J. Chem. Phys.* **126**, 014101 (2007).